2017-04

Experimental investigation of different geometries of fixed oscillating water column devices

Vyzikas, T

10.1016/j.renene.2016.11.061
Renewable Energy
Elsevier BV

Experimental investigation of different geometries of fixed Oscillating Water Column devices

Thomas Vyzikas[a,1], Samy Deshoulières[b], Matthew Barton[a], Olivier Giroux[c], Deborah Greaves[a], Dave Simmonds[a]

[a] *University of Plymouth, School of Marine Science and Engineering, Drake Circus, PL48AA Plymouth, UK*
[b] *Ecole Centrale de Marseille, 38 Rue Frédéric Joliot Curie, 13013 Marseille, France*
[c] *Ecole nationale supérieure des mines de Nantes, 4 Rue Alfred Kastler, 44300 Nantes, France*

Abstract

Oscillating Water Columns (OWCs) are some of the most-studied wave energy converters (WECs). Previous work showed that the geometric characteristics of the OWC can play a significant role in the efficiency of the device. In this study, we investigate the behaviour of different designs of OWC making geometric modifications to the classic design of OWC and the U-OWC, initially suggested by Boccotti [1]. The multi-chamber OWCs examined here are fixed on the seabed and have a slit opening at the seaward side. The physical modelling was undertaken in the COAST laboratory of the University of Plymouth. The devices were tested in regular and irregular wave conditions, with and without power take-off (PTO) mechanism, essentially also testing absorbing seawalls. The aim of the study is to present a preliminary comparison related to the geometry of OWCs under some typical wave conditions and suggest potential shape improvements towards an overall optimization of the devices that takes into account both the hydrodynamic efficiency of the OWC and other design aspects, such as the wave run-up. The present study also endeavours to highlight potential benefits from incorporating OWCs in coastal defence as absorbing seawalls.

Keywords: OWC, U-OWC, tank testing, hydrodynamic efficiency, geometric

[1] Corresponding author, Email address: thomas.vyzikas@plymouth.ac.uk

optimization, absorbing seawalls

1. Introduction

As energy consumption increases globally and environmental issues threaten the quality of life, new sustainable ways of energy generation are actively being researched. Among them, marine renewable energy (MRE) appears to be a viable alternative [2]. MRE includes various technologies, such as wave, tidal, offshore wind and thermal energy. At the moment, only offshore wind power and, to a lesser extent, tidal power are considered mature technologies and receive sufficient investments. On the other hand, emerging wave energy technologies are currently not economically competitive, but still attract engineering interest thanks to the high power density of sea waves and its potential exploitation [3]. In the recent past, the wave energy industry has faced important failures that have delayed the expansion of these technologies. For example, the device installed in Toftestallen was destroyed by a storm in 1998 after six years of good operation [4]. The hybrid pier in Mutriku faced serious damages by severe storms (2007-2009), mainly at uncompleted OWCs [5], possibly due to the non-monolithic design of the chambers and imperfections at the construction stage [6]. After maintenance and modifications though, the Mutriku plant is a good working example of the OWC technology, covering the needs of 100 households. Morever, the icon of the MRE industry, "Pelamis", went to administration in late 2014, having issues securing funding for future developments. It became clear that research is needed for creating robust and efficient devices, in order to boost the development of the wave energy industry [7] and to identify collateral benefits of the use of MRE technologies in sea defences.

Out of the hundreds of patents of WECs registered worldwide, OWC technology appears to be one of the most successful, reaching the stage of full-scale prototypes [8] [9]. On the one hand, there are offshore devices located in deep water, where the available wave power is relatively high. These offshore OWCs are in general floating devices, developed for the first time by Masuda and

commercialized in Japan in 1965 [10]. The first theoretical model of a floating OWC was established by McCormick [11] and recently a 1:4$^{\text{th}}$-scale buoy converter was deployed in Galway Bay, Ireland [12]. On the other hand, there are onshore devices located along the coast in shallow water that are exposed to lower energy potential, unless there are some local energy focusing effects, e.g. due to topography. In fact, around 70% of the energy available in deep water waves is lost through bottom friction as the waves approach the shore [13]. However, onshore or nearshore OWCs have some advantages compared to offshore OWCs: *i*) mooring lines and wet power-transmission cables are not required, *ii*) they operate in a safer sea environment, which increases their survivability, *iii*) they can be more easily accessed and maintained and *iv*) they can serve a dual purpose: electricity generation and coastal protection [14]. The latter is a considerable advantage for OWCs embedded in breakwaters, since the added benefits will increase the viability of such a project by setting a cost-sharing basis.

In its classic form, an onshore OWC system consists of a partially submerged hollow structure, where an underlying water column coexists with an overlying air one, which is connected to the atmosphere with a duct. A submerged seaward opening allows water to flow into the OWC causing internal water oscillation. Subsequently, the water oscillation drives the motion of air and energy can be converted to useful power through a PTO mechanism, usually in the form of a bi-directional air turbine placed in the duct, e.g. Wells turbine. An alternative to the conventional OWC is the U-OWC device [1], which incorporates an additional seaward wall. The U-shape structure appears to be more efficient that the classic OWC shape for realistic sea states, where wind waves and swells coexist, without the need of latching control. As a consequence, the U-OWC is able to resonate in greater frequency bandwidth than the original OWC.

OWC devices have been examined extensively with physical, theoretical, and numerical models. Some milestone experimental studies of OWCs can be found in the literature [15] [16] that are commonly used for comparisons and validation of numerical models in more recent studies [17] [18] [19]. Other

benchmark studies were undertaken by Evans & Porter [20], who developed a theoretical model based on potential theory, to explore the interaction of an OWC with incident waves and to determine its hydrodynamic efficiency. An analytical description of a U-OWC under the assumption of linear wave theory was suggested by Boccotti et al. [21] and was further developed to include a more accurate description of the wave field and the dynamics of the device [22]. Advanced experimental studies of OWCs employed the particle image velocimetry (PIV) technique for acquiring better insight into the hydrodynamics of the OWC [23] [24] and the air motion in the chamber [25]. Commonly, recent work focuses upon the need for validation of numerical models, such as spectral models [26] or computational fluid dynamic (CFD) solvers [27] [28] [29], and the acquisition of appropriate experimental datasets for that scope.

Recognizing the important steps taken by Boccotti [30] in achieving improved performance via geometric optimization of OWCs, the experimental work presented here examines four different OWC geometries, which consist of three rectangular chambers and have alternative external design. The behaviour of these OWCs is investigated in regular and irregular wave conditions, showing how the suggested modifications influence the performance of the devices, the oscillation of the water columns, the run-up on the front wall and the relative motion in the individual chambers. The scope of the work is to show an initial qualitative comparison between the four devices in some typical wave conditions. A companion study referring to the validation of the CFD model OpenFOAM using the present datasets can facilitate the examination of the hydrodynamic characteristics of the OWCs in more detail [31].

In the present study, the devices were tested with and without PTO, since OWCs can potentially operate as absorbing seawalls offering additional advantages to the classic coastal protection structures [32]. The possible merits of using OWC embedded in breakwaters include reduced wave run-up and use of less material for the construction of caissons. However, the high level of noise produced by the turbine is usually a serious consideration for using OWCs near inhabited areas and touristic marinas [6]. Also, the cost of the mechanical and

electrical equipment, regarding the turbine system, cannot be considered insignificant, affecting the attractiveness of the devices to new investors. In the current stage of development of MRE, even prototypes without PTO might be helpful in gaining engineering experience to avoid future failures.

In the remainder of the paper, the description of the devices and the experimental conditions are presented in Section 2. The experimental results for the four devices and the different wave conditions are shown in Section 3. Finally, conclusions and suggestions for future work are drawn in Section 4.

2. Laboratory Methodology

2.1. Models' design

2.1.1. Four variants of OWC

As mentioned in the introduction, the tests reported here focus on four variants of three-chamber OWC models with and without a PTO, which are hereafter referred as "lid-on" and "lid-off" models, respectively. The PTO is simulated by a lid with a circular orifice. The schematic of the four variants shown in Figure 1 illustrates the common characteristics of the devices, which are the internal dimensions of the OWC, in particular the width of the chamber and the height of the air column, and the size of the orifice, which causes the same damping for all the lid-on cases.

Model 1: After studying many different concepts [1] and after parametric optimization [21] [33], Boccotti proposed an improved design of an OWC that has greater resonant bandwidth thanks to its U-shape, allowing it to exploit the energy of both swells and wind waves [30]. A small-scale prototype of this device was tested also in field conditions at the Natural Ocean Engineering Laboratory (NOEL) [34] and full-scale models are under construction in Civitavecchia port [35]. Two other projects have also been approved for the Marina di Cicerone and the Commercial port of Salerno. In the present study, the configuration of the U-OWC tested in NOEL was adopted [34], representing Model 1 in Figure 1.

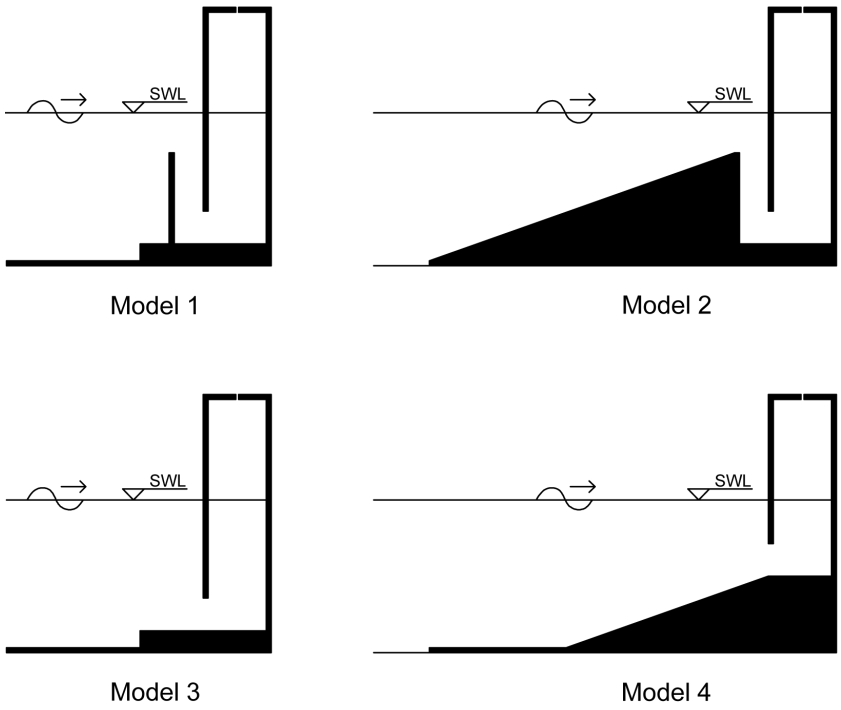

Figure 1: The four lid-on devices studied in the experimental tests. *SWL=still water level

Model 2: This model in Figure 1 resembles the U-shape of Boccotti's design [34], but it is fronted by a submerged slope representing part of the toe or armour section of a real breakwater. This slope has a gradient of 1:2.5, which is a typical value for rubble-mound breakwaters, and it expands from the highest point of the submerged wall to the seaward side. The scope of this modification is to examine the impact of an armoured slope or a toe protection structure on the hydrodynamic characteristics of the OWC. Realistic studies of OWCs should consider such a sloping structure in front of the main structure for toe protection, especially because WECs are designed to operate in energetic sea climates. In any case, sediment transport and debris accumulation tend to create inclined features on the bed in front of such structures over long periods of time [36].

Model 3: This model refers to the conventional design of the OWC shown as

Model 3 in Figure 1. It is probably the device with the simplest geometry, comprising a vertical seaward wall with a horizontal slit opening at the bottom. This type of device has been extensively studied experimentally [16] and numerically [37], as mentioned in the Introduction. Prototypes have also been constructed and operated in sea for a number of years, such as the PICO [9] and LIMPET device [8]. Compared to previous studies [27] [17], the present work examines conventional OWCs with higher draught of the front wall and high damping. This geometry was considered in order to be consistent with Boccotti's design of the U-OWC [34] and allow for direct comparisons to be drawn. The high damping in combination with the relatively high waves tested here results in high air pressure in the OWC chambers, making the present study challenging.

Model 4: An alteration of the conventional design, referred to as Model 4 in Figure 1, was also examined following the same principles of toe protection as for Model 2. A similar configuration has been tested in approximately 1:6^{th} of the present scale by Koola et al. [38]. Model 4 has a shorter draught of the seaward wall, but the same slit opening as Model 3. Note that, the bottom of the chambers is raised inside the OWC, so that it is at half of the water depth, similar to the conventional OWC model suggested by Boccotti [30]. The slope in front of the device is again 1:2.5. The scope of testing Model 4 is to examine the influence of a different draught, keeping the seaward slit opening constant. At the same time, the effect of the toe protection can be examined through comparison with Model 3.

2.1.2. Model scaling

The 35m long flume of the COAST laboratory at the University of Plymouth [39], where the experiments took place, has a maximum operational depth of 0.75m and width of 0.6m. The flume is equipped with an absorbing piston-type wave paddle that is capable of generating regular and irregular waves. The OWCs were placed before the other end of the flume with the back wall of the structure at a distance of 28m from the wave paddle. All the walls of the flume are transparent allowing visual observations. The experimental set-up is

presented in Figure 4.

The scaling of the present model was based on the water depth ratio between Boccotti's small-scale field experiments [34] and the maximum available water depth of COAST's flume. Boccotti's model was located at a water depth of 2.1 m, therefore the model had to be scaled down to fit into the depth of 0.75 m of the present flume. The OWC was scaled by Froude dynamic similarity [40], since gravity waves are examined with wavelengths much larger compared to the wave heights and the viscous forces on water surface motion inside the device are small. Therefore, the geometric scaling factor obtained from the two water depths is:

$$s_f = \frac{\text{Length of prototype}}{\text{Length of model}} = \frac{2.1}{0.75} = 2.8 \tag{1}$$

Based on s_f, the scaled geometric characteristics of the OWCs are listed in Table 1. The parameters of this Table are shown in the generic schematic of the devices, referring to Model 1, in side view (Figure 2) and plan view (Figure 3). It can be seen that the OWCs are symmetrical to the centreline of the flume, and thanks to this symmetry, 2-dimensional tests in a flume can be conducted for uni-directional waves. The devices were manufactured from marine plywood with all the intersections bonded and sealed with silicon filler for ensuring airtightness.

h_d	w_1	w_2	w_3	s_o	c_1	c_2
0.750	0.554	0.518	0.107	0.161	0.644	2.000
b_1	b_2	k_w	o_r	l_1	l_{tot}	
0.143	0.286	0.024	0.015	0.184	0.600	

Table 1: Size of geometric parameters of the present OWC device in (m).

2.1.3. Power Take-Off

The conversion of the pneumatic energy of the air in the OWC chambers to electricity is performed by a PTO mechanism, which in the case of OWCs,

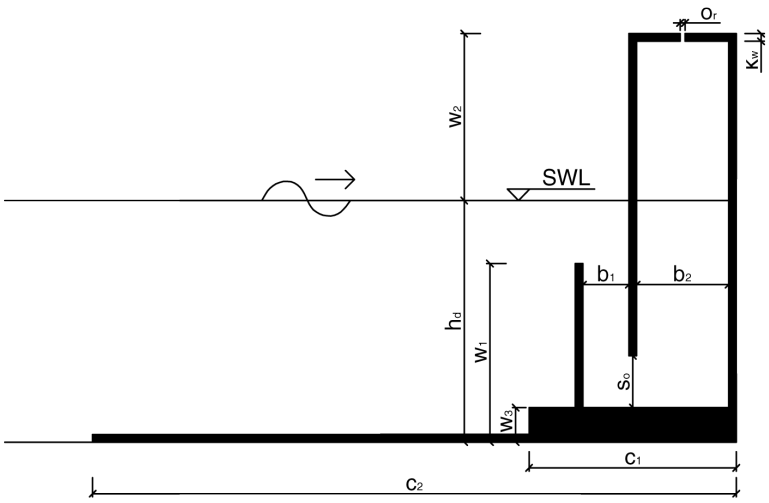

Figure 2: Side view of the U-OWC with the geometric parameters used.

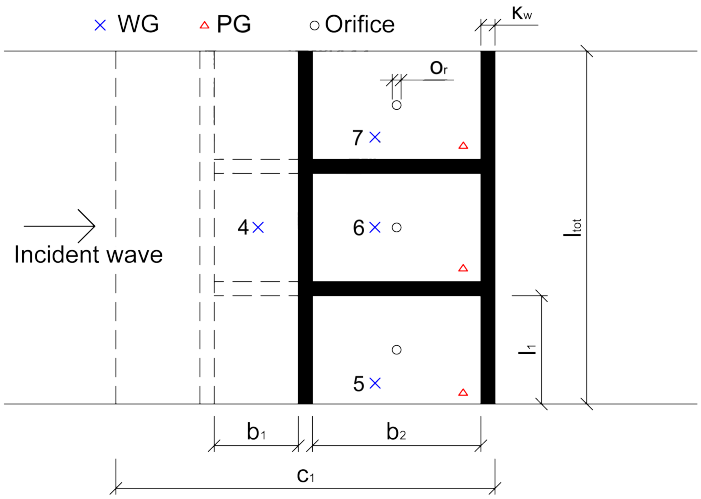

Figure 3: Plan view of the experimental model displaying the locations of the pressure gauges (PG), wave gauges (WG) and orifices.

is usually a bi-directional Wells turbine [41]. Due to scaling differences and modelling difficulties in the laboratory, a scaled turbine is not usually practical. However, its damping effect has to be reproduced, since it alters the hydrodynamic behaviour of the device. Using an orifice is a well-established method for that scope [42] [43]. The size of the orifice determines the magnitude of the damping. In the present study, a circular orifice was placed in the lid at the top of each chamber of the OWC. Its diameter of 1.5 cm was scaled on Boccotti's design [34] to achieve an orifice of 0.35% of the total plan area of each chamber. All the OWC variants were tested with the same circular orifices, as shown in Figure 3. The damping due to the small orifice is higher compared to similar previous studies, where the orifice covered 2.7% - 14.7% [28], 0.78% - 7.8% [43] and 0.78% - 3.91% [27] of the plan area of the chamber, resulting in significant internal air pressure.

The same devices were tested without a PTO by completely removing the lid. The lid-off results can only be used for examining absorbing seawalls and not WECs, since the inclusion of a PTO alters the eigenfrequency of the device and consequently its hydrodynamic response and performance. Nonetheless, the comparison between OWCs with and without PTO presented in Section 3 reveals interesting information regarding the wave dissipation and general behaviour of the devices for potential other uses as elements of breakwaters..

2.2. Experimental design

2.2.1. Instrumentation and data acquisition

The free surface elevation was recorded with seven resistive wave gauges (WG) at a sampling frequency of 128 Hz. After testing each model, the WGs were recalibrated for greater confidence. Between the wave tests, the free surface was allowed to settle for approximately five minutes, in order to avoid any spurious effects from long or cross-shore waves remaining in the flume. The positions of the WGs are shown in Figures 3 and 4, with WGs 1-4 located upstream of the OWCs along the flume centreline and WGs 5-7 placed inside each one of the three chambers. The first three WGs were used to measure the inci-

dent waves for quality control of the results and later for the reflection analysis (see Section 3.2.1). WG 4 was used to measure the water elevation just in front of the devices, which is practically associated with the run-up on the front wall of the OWCs. WGs 5-7 were placed at different offsets from the side walls of each chamber (see Figure 3), in order to examine the possibility of internal waves (sloshing) or distrubances inside the chambers, by comparing the phase differences from the recoordings. Of course, sloshing can be observed better with more than one WG in the same chamber, but thanks to the symmetry of the chambers, the present layout of the WGs allows for such studies.

For the lid-on tests, a pressure gauge (PG) was mounted on the lid of each chamber to measure the pressure variations in the chamber, as shown in Figure 3. The recorded pressure was used for the calculation of the power absorbed and capture width of the device. The sampling frequency of the PGs was also 128Hz and the recording was sychronised with the WGs.

The wave generation was performed by a piston wave paddle, which was computer-controlled with a linear transfer function. Absorption was achieved through a force feedback mechanism [44]. A ramp-up time of approximately one wave period was selected at the paddle control to facilitate the smooth generation of the first waves in still water.

To assess the laboratory errors, a repeatability evaluation was performed using regular waves and Model 1. Each test was repeated five times with Model 1 lid-on. The first test was used as a reference measurement and the error for

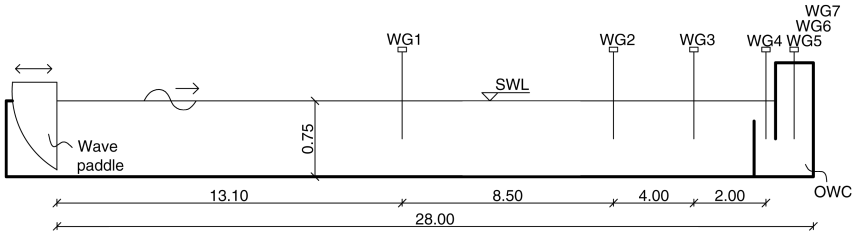

Figure 4: Experimental set-up indicating the locations of the wave gauges (WG) relative to the OWC and the wave paddle. Dimensions in (m).

each test was calculated as the mean value of the absolute difference between the corresponding peaks of the two examined timeseries over the wave height, as seen in Equation 2. The wave height is calculated as the mean value of the difference between the elevations of the crests and the neighbouring troughs recorded in the windowed timeseries after the ramp-up waves and before the arrival of reflections. The total error for each wave is calculated as the mean value of the errors from the four comparisons with first test. The average error for all the regular wave tests was approximately 1%, indicating that the results are consistent and repeatable.

$$Error = \frac{1}{N}\sum_{1}^{N}\frac{\overline{|recording\,1 - recording\,i|}}{\overline{wave\,height}}100\% \tag{2}$$

2.2.2. Wave characteristics

The four devices were tested with and without PTO under four regular and four irregular wave conditions. The characteristics of the regular waves are shown in Table 2, referring to the analysed values from the obtained timeseries with H and f being the wave height and frequency, respectively. For each wave, the recorded signal from WGs 1-3 was windowed to remove the ramp-up of the paddle and the reflections from the OWC. This method is preferred for determining the incident wave characteristics, instead of using the input values to the wave paddle, because it eliminates any potential discrepancies induced by the calibration and it provides more accurate input for the calculations that follow.

The initial selection of the waves was based on the natural frequency of the OWC, which can be estimated from the draught of its front wall [45], as seen in Equation 3. According to Equation 3, the natural frequency of Model 3 is approximately 0.51 Hz. It was decided to examine two other lower wave frequencies and a higher wave frequency, in order to cover sufficient frequency

bandwidth.

$$f_c = \frac{1}{2\pi}\sqrt{\frac{g}{L_1 + L_2}} \tag{3}$$

where L_1 is the draught of the front wall of the OWC and L_2 is an effective length due to the added mass induced by the PTO, here approximated as equal to L_1.

Each regular wave test had a duration of 30 s, essentially assessing 4-7 wave periods, depending on the case. For the given water depth, these heights and periods correspond to intermediate depth second order waves [46]. The range of wave periods and heights was selected in order to examine waves around the resonant frequency of the OWCs, with different steepness.

	Regular waves		Irregular waves	
Wave	H (m)	f (Hz)	H_s (m)	f_p (Hz)
1	0.122	0.570	0.066	0.651
2	0.096	0.510	0.057	0.602
3	0.088	0.465	0.056	0.551
4	0.159	0.385	0.077	0.445

Table 2: Regular and irregular wave characteristics

The wave characteristics of the four irregular waves tested are also shown in Table 2, with H_s and f_p being the significant wave height and peak period of the measured spectrum in the flume, respectively. A Joint North Sea Wave Project (JONSWAP) [47] energy spectrum was chosen as an input spectrum at the wave paddle, since this type of spectrum represents a widely used energy distribution in industry. Its equation relating H_s and f_p is given in Equation 4 and it can be derived from the basic equation [46] using $H_s = 4\sqrt{m_0}$ and $m_0 = \alpha g^2 \omega^{-4}(0.06533\gamma^{0.8015} + 0.13467)$, with m_o being the zeroth moment of

the spectrum and α a spectral parameter.

$$S_{jon}(f) = 0.205 H_s^2 f_p^4 f^{-5} exp\left(-\frac{5}{4}\left(\frac{f_p}{f}\right)^4\right)\gamma^r \quad (4)$$

where f is the discrete frequency of each wave component, γ (= 3.3) the JONSWAP spectral peak enhancement parameter and $r = \exp[-\frac{(f-f_p)^2}{2f_p^2\sigma^2}]$, with $\sigma = 0.07$ for $f \leq f_p$ or $\sigma = 0.09$ for $f > f_p$.

The energy spectrum was generated by the wave paddle with linear superimposition of 200 wave components with assigned random phases between 0 and 2π rad. A low and high cut-off frequency corresponding to 0.2 Hz and 1.5 Hz, respectively were used to limit the wave generation to wave components with meaningful energy only. The repeat interval of the signal was 180 s.

The values for irregular waves in Table 2 were obtained after analysing the recorded timeseries of the surface elevation by means of reflection analysis, as described in Sections 3.2.1 and 3.2.2. These values were selected in order to correspond to relatively mild wave condition in the South West of England [48] and to have f_p close to the resonance frequency of the examined OWCs. The H_s and f_p values were scaled based on the water depth, taken as 10 m in full scale, using Froude similarity with a scale of approximately 1:13.

3. Results and discussion

3.1. Regular waves

3.1.1. Relative surface elevation at characteristic locations

The results of the surface elevation are examined at two characteristic locations of the OWC, namely inside the central chamber and at the front wall, measured with WG 6 and WG 4, respectively. The surface elevation is normalised by the incident wave height and it is used here to observe the general response of the OWC models, useful for the design. Commonly, the non-dimensional Response Amplitude Operator (RAO) is employed, which is defined for one degree

of freedom, i.e. vertical oscillation, by the non-dimensional ratio of amplitudes without considering the phases [49] as:

$$RAO(f) = \frac{\Xi}{\alpha_w} \tag{5}$$

where Ξ represents the amplitude of the response of the water surface in the chamber of the OWC and α_w the amplitude of the incident wave, which, to good approximation, is taken as half of the wave height (H).

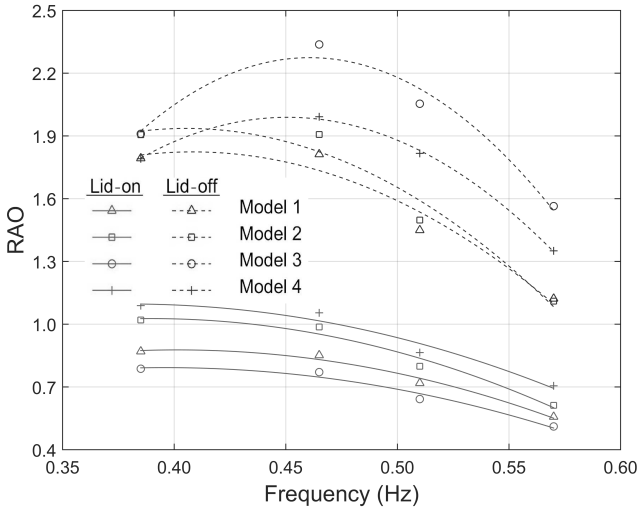

Figure 5: Relative surface elevation inside the central chamber of each lid-off (- -) and lid-on (–) device for the four regular wave conditions.

Figure 5 presents the RAO in the central chamber of each device for the lid-on and lid-off configurations for the four regular waves tested. A second order polynomial fitting is plotted to facilitate comparison of the results. The central chamber is selected as a representative case, since for most of the waves and devices tested, the behaviour of the three chambers is similar, as discussed in Section 3.1.3.

The effect of the damping induced by the PTO can be clearly observed, since the RAO of the lid-on OWCs is around half that of the lid-off OWCs, as might be anticipated. Moreover, the shape of the curves indicates a possible resonance

at approximately 0.45 Hz for the lid-off models and at a lower frequency for the lid-on models. However, this is hard to confirm due to the limited range of the frequencies examined. It can be seen that Equation 3 with $L_1 = L_2$ overestimates the resonant frequency of the OWCs, possibly due to the high damping of the PTO, which results in greater added mass.

An interesting observation from Figure 5 refers to the relative behaviour of the four models, which is substantially different between the lid-on and lid-off cases. The conventional design (Model 3) appears to have the highest RAO in the absence of lid and the lowest when the lid is present. The same trend appears for Model 4, which is a modification of Model 3. On the other hand, Models 1 and 2 have the two lowest RAO for the lid-off configuration and the two highest for the lid-on configuration. This indicates that the extra submerged seaward wall of U-OWCs significantly alters the hydrodynamic behaviour of the device compared to the conventional OWCs. Another important observation is that the U-OWC with the ramp (Model 2) has higher RAO compared to the standard U-OWC, irrespectively of the presence of the lid.

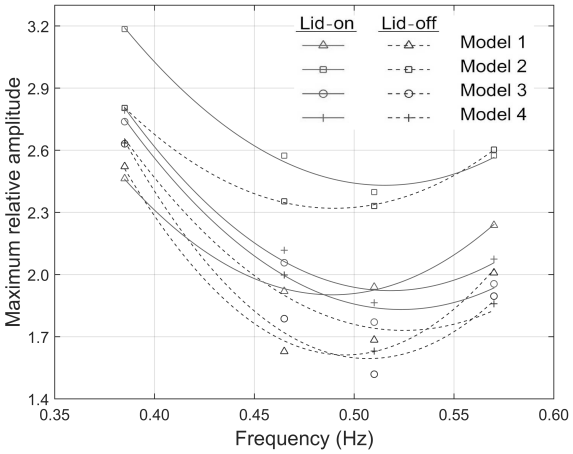

Figure 6: Relative surface elevation at the front wall (WG 4) of each lid-off (- -) and lid-on (–) device for the four regular wave conditions.

The second characteristic location refers to WG 4 upstream of the front

wall of the OWCs, which can be used to examine the run-up on the front wall. Figure 6 shows the run-up for all the lid-on and lid-off devices under the four regular wave conditions, normalized by the incident wave amplitude. Run-up is calculated as the average of the maxima of surface elevation recorded in every wave test. A second order polynomial fitting is plotted for ease of comparisons.

In general, Figure 6 shows that the run-up is higher for the lid-on cases when examining a specific device. Additionally, Model 2 has significantly higher run-up compared with the other models, which is presumed here to be an effect the shoaling caused by the ramp. The same can be observed for Model 4 when compared to Model 3, but since the draught of the front wall is different and the slope is shorter, no immediate conclusion should be drawn. The conventional U-OWC (Model 1) has small run-up for the low-frequency waves only, while the conventional OWC (Model 3) induces low run-up for the whole range of frequencies tested.

Run-up might be an important restriction when designing marinas and ports, causing operational problems in cases of over-topping. The run-up on a fully reflective vertical breakwater is approximately two times the incident wave amplitude. Thus, for the majority of the tests in Figure 6, excluding Model 4 and the lowest-frequency wave, a breakwater with embedded OWCs should behave better than a conventional vertical breakwater, with lower likelihood of over-topping.

3.1.2. Hydrodynamic efficiency

The most important parameter when examining the performance of an OWC is the hydrodynamic efficiency, which is defined as the ratio of the power absorbed by the OWC (P_{abs}) over the incident wave power (P_{inc}) per meter width of the device, as seen in Equation 6. The hydrodynamic efficiency is also referred in the literature as capture width ratio (C_w) [45], and of course it is calculated for devices with PTOs only.

$$C_w = \frac{P_{abs}}{P_{inc}} \tag{6}$$

The incident wave power is given by the total incident energy, i.e. the summation of kinetic and potential energy, per time unit and per meter length of the wave crest, as shown in Equation 7 [45]:

$$P_{inc} = \frac{1}{8} w \rho g H^2 c_g \tag{7}$$

where w the transverse width of the wave tank, which corresponds here to thwidth of the chambers (l_1 in Table 1), ρ the density of the water, g the gravitational acceleration and c_g the wave group celerity, given as $c_g = \frac{\omega}{\kappa}\frac{1}{2}\left(1 + \frac{2\kappa h}{\sinh(2\kappa h)}\right)$, with ω being the angular frequency of the wave, h the depth of the flume and κ the wave number.

For the calculation of the power absorbed by the OWC, the timeseries of the free surface displacement and pressure are required. The power absorbed by the device is calculated by the energy absorbed in one wave cycle divided by the wave period (T), as shown Equation 8:

$$P_{abs} = \frac{1}{T} \int_0^T p(t)\, v(t)\, S_c\, dt \tag{8}$$

where $p(t)$ the instantaneous air pressure inside the chamber and $v(t)$ the instantaneous velocity inside the chamber, calculated by the time derivative of the free surface displacement in the device. S_c is the section of the chamber, given by its internal dimensions, namely $b_2 \times l_1$ (see Table 1).

Figure 7 presents the hydrodynamic efficiency of the four devices under the four regular conditions, calculated from the recordings in the central chamber. A second order polynomial fitting is also used for easier comparisons. Considering the shape of the curves and the large variation of C_w, it seems that the waves tested cover the frequency region around the maximum performance of the devices, which gives added value to the present results.

The results of Figure 7 are somewhat comparable with those for the RAO of the lid-on devices in Figure 5, confirming that the presence of the ramp alters the hydrodynamics of the OWCs and improves the performance, since Model 2 and Model 4 have higher values of C_w than Model 1 and Model 3,

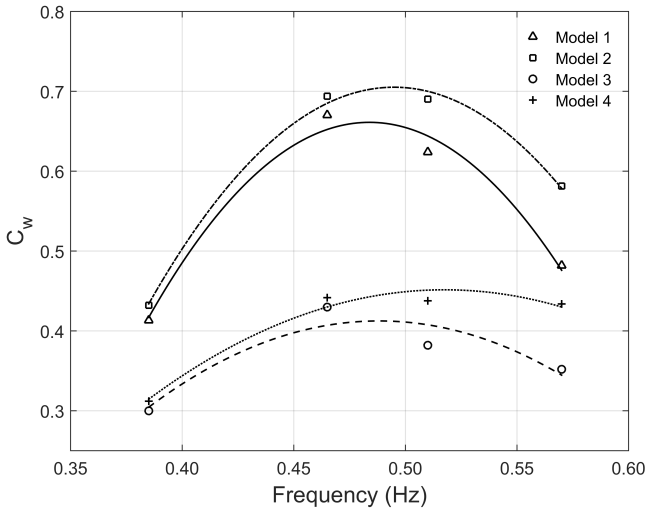

Figure 7: Capture width for the central chamber of each device for the four regular waves.

respectively. The most important aspect of the results regarding the C_w, is the significant improvement in the performance of U-OWCs (Models 1 and 2) compared to conventional OWCs (Models 3 and 4), especially close to the peak of the performance curve, where C_w is almost twice as high.

3.1.3. Comparison between the chambers

As stated in Section 2.1 all the OWC devices had three identical chambers, which were not connected. Therefore, the chambers are expected to respond independently to the incident waves and in theory, they should have identical behaviour. Here, the relative response of the three chambers of the lid-off devices is examined for all the regular waves. The comparison between the chambers is performed by means of RAOs, similar to the analysis in Section 3.1.1. The lid-off devices are selected for this test, because they have higher RAOs compared to the lid-on devices and their results are not influenced by imperfections in the manufacturing of the lid.

The results are shown in Figure 8, where the markers indicate the different models and the colours refer to each of the four regular waves. If a line is

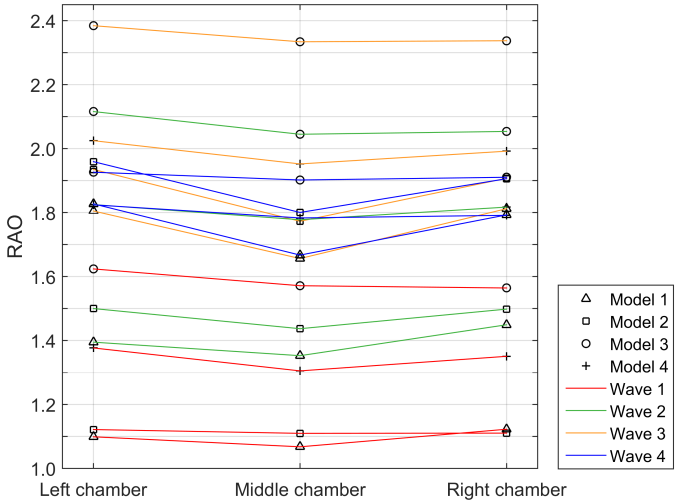

Figure 8: RAO of the three chambers for the lid-off devices under the four regular waves.

horizontal, the chambers behave exactly the same. The left, middle and right chamber here refer to the bottom, central and top chambers in Figure 3, with recordings taken from WG 5, WG 6 and WG 7, respectively. The present results indicate that the behaviour of the three chambers is not identical. It should be noted that this does not seem to be an effect of the layout of the internal WGs, which were located in such a way (see Figure 3), in order to observe possible sloshing or any other distrurbances of the free surface inside the chambers. The examination of the timeseries of the surface elevation showed that the internal oscillation had the same phase for all the three WGs in the chambers.

In particular, the behaviour of the three chambers is similar for Wave 1 and it has more discrepancies for Wave 4, which indicates that there is a potential correlation between the wave length and the differences in RAO between the chambers. Moreover, Models 1 and 2 seem to have noticeably higher RAO of the side chambers compared to the central one, especially for the longer waves (Waves 3 and 4). The same is not the case for Models 3 and 4, where the behaviour of the chambers is more consistent. This indicates that the presence

of the submerged wall of the U-OWCs alters the hydrodynamic characteristics of the flow and results in different RAOs for the chambers. One can argue that the side walls of the flume can potentially alter the behaviour of the side chambers in comparison to the central one, but despite the fact that the problem is symmetrical, these chambers did not exhibit always consistent behaviour for all the cases tested here. Further examination of the flow patterns in the vicinity and inside the devices is required for explaining the different behaviour of the chambers.

3.2. Irregular waves

3.2.1. Data processing

The analysis of irregular waves with random phases requires special processing of the results in order to remove the reflections and create a smooth spectrum, which is easier to interpret.

During the 180 s of each irregular wave test, there are many reflected waves from the OWC and some re-reflected waves from the wave paddle, which contaminate the recorded signal. The accurate assessment of the performance of the devices requires the extraction of the incident wave field from the measured timeseries. This can be achieved by means of reflection analysis. A two-WG method [50] was employed here, using the recordings of the surface elevation from WG 2 and WG 3. This option was considered the best, since the distance between WG 1 and WG 2 is much longer and WG 4 is subject to local flow disturbances caused by the OWC. Common practice suggests short distance between the WGs used for reflection analysis of approximately 10-20 cm. However, trial of the method to synthetic data and numerical model results [31] demonstrated that even for much longer distances between the WGs, e.g. 1-4 m, the shape and the energy of the incident spectrum can be accurately predicted. Increasing the distance between the WGs mainly affected the phasing of the wave components, resulting in discrepancies in the observed surface elevation.

The estimation of the spectral properties was achieved though segmentation and averaging of the spectrum obtained after the reflection analysis, in order

to yield a smoother spectrum for better interpretation of the results [46]. This is common practice to avoid the "noisy" appearance of a spectrum obtained by fast-Fourier transform (FFT). The recorded signal is subdivided to p_n segments and subsequently, the frequency resolution of the resulted spectrum is reduced by p_n times, yielding an error of this process of $\frac{1}{p_n}100\%$. The optimal number of segments is selected by trials and for the present case was $p_n = 8$. The smoothing method ensures that the total energy between the measured and the processed spectrum is conserved. In practice, the smoothing method for the spectra, as described in the appendix of [46], is the same as the commonly used Welch without overlapping of the segments. Finally, it was decided to use the method of [46], since it has no bias on the selection of the overlapping window function, as with Welch method, and the frequency resolution was sufficient for the scope of the present study

The resulted incident spectra after the reflection analysis and smoothing are presented in Figure 9. The comparison with the input spectra to the wave paddle revealed some discrepancies, possibly caused by the calibration and the imperfect reflection absorption of the wave paddle. The peaks of the measured spectra were lower than the theoretical and energy was spread to higher frequencies. Despite these differences, the spectral shape was maintained to an acceptable degree and the measured incident spectra had on average 20% higher energy than that of the corresponding input spectra. In the analysis of the behaviour of the OWCs that follows, the processed incident spectra were employed for better reliability.

Figure 9 also shows that in spite of the different random phases of the irregular waves and the long distance between the WGs used for the reflection analysis, the obtained incident spectra for all the models were very similar. A small difference close to the peak frequency was observed for irregular Wave 1, where the models with the slope appeared to receive more incident energy than the conventional OWC and U-OWC (Models 1 and 3). The reason for this is not clear, but it is assumed to be an artefact of the reflection analysis or the effect of nonlinearities caused by the devices, such as the reflection from the

ramp. Similar behaviour can be observed, to a lesser extent, for irregular Wave 2, while the curves collapse to one for irregular Waves 3 and 4 that have lower peak frequencies (see Table 2).

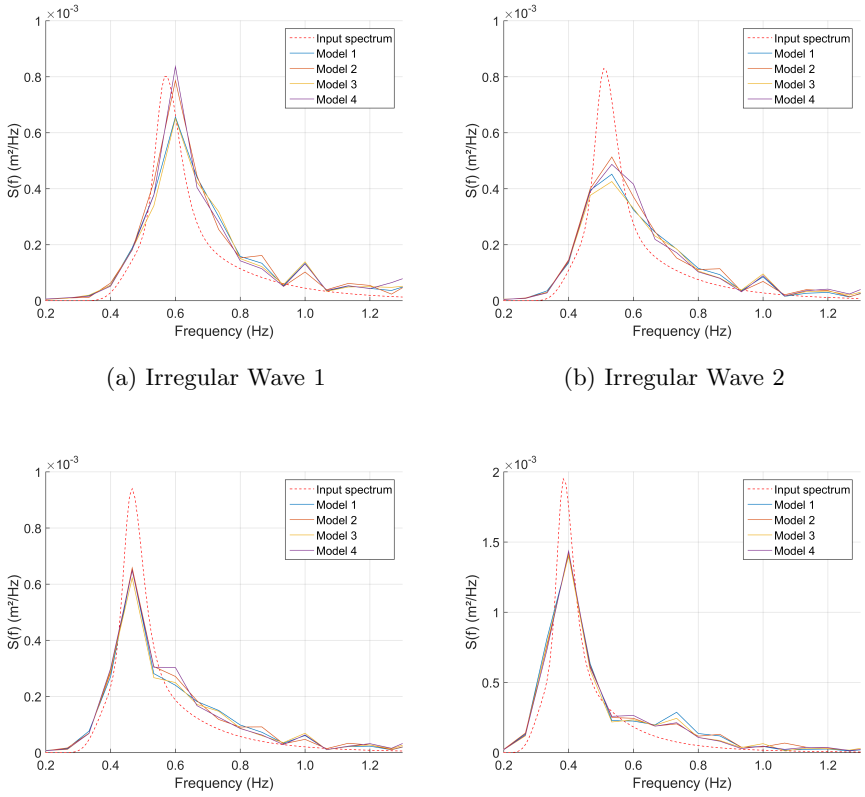

(a) Irregular Wave 1

(b) Irregular Wave 2

(c) Irregular Wave 3

(d) Irregular Wave 4

Figure 9: Calculated incident spectra for every model under the four irregular wave conditions.

3.2.2. Hydrodynamic efficiency

Similar to the regular waves, the calculation of the hydrodynamic efficiency for the irregular waves (C_w^{irr}) requires the incident power of the wave field, which can be found by the zeroth spectral moment of the variance energy density of the incident spectrum [51] obtained after the reflection analysis. The incident

wave power per meter length reads:

$$P_w^{irr} = \rho g \int_0^\infty c_g(\omega) S(\omega)\, d\omega \tag{9}$$

The absorbed power by the OWC (P_{abs}^{irr}) is calculated similarly to Equation 8 for the length of the time series, between the arrival of the first waves at the OWC at time t_0 and the end of the signal at time t_l:

$$P_{abs}^{irr} = \frac{1}{t_{tot}} \int_{t_0}^{t_l} p(t)\, v(t)\, S_c\, dt \tag{10}$$

C_w^{irr} can now be found by the ratio of the absorbed energy E_{abs}^{irr} over the incident wave energy E_w^{irr} between times t_0 and t_l.

$$C_w^{irr} = \frac{E_{abs}^{irr}}{E_w^{irr}} = \frac{\int_{t_0}^{t_l} p(t)\, v(t)\, S_c\, dt}{w\,(t_l - t_0)\, P_w^{irr}} \tag{11}$$

Following this procedure, a value of the C_w^{irr} was calculated for every irregular wave and model. To allow comparison, each value of the C_w^{irr} had to be assigned to a representative frequency for every spectrum. A spectrum is commonly represented by its peak frequency (f_p), which corresponds to frequency of the maximum energy density. However, the relatively low resolution of the smoothed spectra (see Figure 9) can introduce some errors in the estimation of f_p. Therefore, it was preferred to calculate f_p from the spectral moments for greater accuracy. At first, the mean frequency of the spectrum f_{mean} was calculated as the ratio between the first and the zeroth spectral moments, as shown in Equation 12. f_p could be then related to f_{mean} with Equation 13 for a JONSWAP spectrum with $\gamma = 3.3$ [52]. In some cases presented here, $\gamma < 3.3$, however the theoretical value of the coefficient (0.8345) can be taken without important loss of accuracy (see Table 3 in [52]).

$$f_{mean} = \frac{m_1}{m_0} = \frac{\int_0^\infty f E(f)\, \mathrm{d}f}{\int_0^\infty E(f)\, \mathrm{d}f} \tag{12}$$

$$f_p = 0.8345 f_{mean} \tag{13}$$

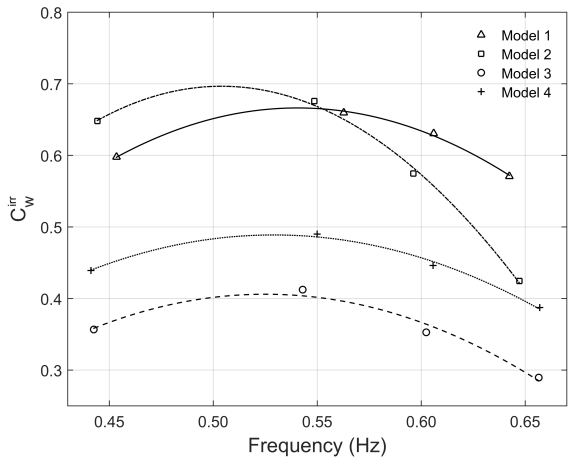

Figure 10: Capture width ratio of the central chamber of each Model for the four irregular waves.

Figure 10 shows the comparison between the C_w^{irr} for the middle chamber of each model. A second order polynomial fitting is used to facilitate comparisons. Similarly to the regular waves in Figure 7, the U-OWCs (Models 1 and 2) seem to be more efficient than the conventional OWC (Models 3 and 4). Moreover, for irregular waves, Model 4 appears to be considerably more efficient than Model 3, possibly because it resonates in higher frequencies, as discussed in Section 3.1.2. On the other hand, Model 4 does not have better performance for all the tests, as it was the case for regular waves. In general, the curvature of the curves for irregular waves is smaller than that of regular waves (Figure 7), which can be explained by the spread of energy over many frequencies.

Even though Figure 10 shows some clear trends in the behaviour of the models, it should be noted that these results come from single tests for each irregular wave with random phases and more experiments are required to minimise the bias of the phases and draw more solid conclusions.

4. Conclusions

In this study, four multi-chamber designs of OWCs were examined with a PTO for energy generation and without a PTO, as absorbing seawalls. Regarding the performance of the devices with the PTO, the experimental results confirmed that the U-OWC, as suggested by Boccotti [30], is superior to the conventional OWC designs. The new U-OWC design with the slope, as suggested here, appeared to have comparatively good performance, which in most cases was better that all the other models. Moreover, the proposed modification to the conventional OWC by including a toe protection unit enhanced the performance of the classic model. Additionally, the response of the devices was examined in terms of RAO inside each chamber and run-up on the front wall of the device. The latter is associated with over-topping, which is a major design consideration for piers and breakwaters of ports. The present results demonstrated that for most of the wave conditions tested the presence of the OWC can reduce the run-up compared with vertical wall breakwaters. The potential merits for using OWC in classic coastal structures can foster the expansion of MRE on a cost-sharing basis with coastal protection.

Future work should examine the different models in more wave conditions and with additional instrumentation, in order to draw in-detail conclusions regarding the effect of the geometric modifications. As demonstrated by the present study, the geometry of the OWC can have significant impact on its behaviour. In future parametric analyses, other design aspects can be examined, such as the draught of the front wall and the internal geometry of the chambers. Different levels of damping and other types of PTOs should also be considered, since the damping, in combination with the geometry of the OWC, determine the performance of the device. Ideally, the type and the damping of the PTO should be tuned for each OWC based on the performance curve and the wave climate that the device will be deployed in. For the case of embedding OWCs in piers of ports, the reflection coefficients of the structure, together with the run-up and overtopping should be studied carefully. Finally, an important de-

sign aspect is the behaviour of the individual chambers and their interactions in unidirectional and oblique waves, as the present results indicated differences in the chambers' response to regular waves.

References

[1] P. Boccotti, On a new wave energy absorber, Ocean Engineering 30 (9) (2003) 1191–1200. doi:10.1016/S0029-8018(02)00102-6.
URL http://linkinghub.elsevier.com/retrieve/pii/S0029801802001026

[2] A. Clément, P. McCullen, A. Falcão, A. Fiorentino, F. Gardner, K. Hammarlund, G. Lemonis, T. Lewis, K. Nielsen, S. Petroncini, M. T. Pontes, P. Schild, B. O. Sjöström, H. C. Sø rensen, T. Thorpe, Wave energy in Europe: Current status and perspectives, Renewable and Sustainable Energy Reviews 6 (5) (2002) 405–431. doi:10.1016/S1364-0321(02)00009-6.

[3] E. Enferad, D. Nazarpour, New Developments in Renewable Energy, Intech, 2013, Ch. 12. doi:10.5772/53806.
URL http://www.intechopen.com/books/new-developments-in-renewable-energy/ocean-s-renewable-power-and-review-of-technologies-case-study-waves

[4] R. H. Charlier, M.-C. Chaineux, C. W. Finkl, A. C. Thys, Power from Artic waters, in: International Congress of Polar Science, no. 42, 2012, pp. 93–102.

[5] E. Medina-Lopez, W. Allsop, A. Dimakopoulos, T. Bruce, Conjectures on the Failure of the OWC Breakwater at Mutriku, in: Coastal Structures & Solutions To Coastal Disasters Joint Conference, 2015, pp. 1–12.

[6] Y. Torre-Enciso, J. Marqués, L. I. Lopez de Aguileta, Mutriku . Lessons learnt, in: 3rd International Conference on Ocean Energy, Bilbao, Spain, 2010.

[7] J. Weber, WEC Technology Readiness and Performance Matrix finding the best research technology development trajectory, in: 4 th International Conference on Ocean Energy, Dublin, Ireland, 2012.

[8] C. B. Boake, T. J. T. Whittaker, M. Folley, H. Ellen, Overview and Initial Operational Experience of the LIMPET Wave Energy Plant, Vol. 3, 2002, pp. 586–594.

[9] A. Pecher, J. P. Kofoed, I. L. Crom, F. Neumann, E. d. B. Azevedo, Performance assessment of the Pico OWC power plant following the EquiMar Methodology, in: Proceedings of 21st International Offshore and Polar Engineering Conference, Vol. 8, 2011, pp. 548–556.
URL http://e-book.lib.sjtu.edu.cn/isope2011/data/papers/11TPC-447Pecher.pdf

[10] A. F. O. Falcão, J. C. C. Henriques, Model-prototype similarity of oscillating-water-column wave energy converters, International Journal of Marine Energy 6 (2014) 18–34. doi:10.1016/j.ijome.2014.05.002.

[11] M. E. McCormick, Analysis of a Wave Energy Conversion Buoy, Journal of Hydronautics 8 (3) (1974) 77–82.

[12] A. F. O. Falcão, Modelling of Wave Energy Conversion, Tech. rep. (2013).
URL https://fenix.tecnico.ulisboa.pt/downloadFile/3779580606646/Chapter%25201%25282014%2529.pdf

[13] D. Stagonas, G. Müller, N. Maravelakis, D. Magagna, D. Warbrick, Composite seawalls for wave energy conversion: 2D experimental results, in: 3rd International Conference on Ocean Energy, Bilbao, Spain, 2010.

[14] T. Hammons, Energy Potential of the Oceans in Europe and North America: Tidal, Wave, Currents, Otec and Offshore Wind, International Journal of Power and Energy Systems 28 (4). doi:10.2316/Journal.203.2008.4.203-4142.

[15] A. Sarmento, Wave flume experiments on two-dimensional oscillating water column wave energy devices, Experiments in Fluids 12 (4-5) (1992) 286–292. doi:10.1007/BF00187307.
URL http://dx.doi.org/10.1007/BF00187307

[16] M. T. Morris-Thomas, R. J. Irvin, K. P. Thiagarajan, An Investigation Into the Hydrodynamic Efficiency of an Oscillating Water Column, Journal of Offshore Mechanics and Arctic Engineering 129 (4) (2007) 273–278. doi:10.1115/1.2426992.

[17] Y. Zhang, Q.-P. Zou, D. Greaves, Airwater two-phase flow modelling of hydrodynamic performance of an oscillating water column device, Renewable Energy 41 (2012) 159–170. doi:10.1016/j.renene.2011.10.011.
URL http://dx.doi.org/10.1016/j.renene.2011.10.011

[18] Y. Luo, J. R. Nader, P. Cooper, S. P. Zhu, Nonlinear 2D analysis of the efficiency of fixed Oscillating Water Column wave energy converters, Renewable Energy 64 (2014) 255–265. doi:10.1016/j.renene.2013.11.007.

[19] D.-Z. Ning, J. Shi, Q.-P. Zou, B. Teng, Investigation of hydrodynamic performance of an OWC (oscillating water column) wave energy device using a fully nonlinear HOBEM (higher-order boundary element method), Energy 83 (2015) 177–188. doi:10.1016/j.energy.2015.02.012.
URL http://linkinghub.elsevier.com/retrieve/pii/S0360544215001644

[20] D. Evans, R. Porter, Hydrodynamic characteristics of an oscillating water column device, Applied Ocean Research 17 (3) (1995) 155–164. doi:10.1016/0141-1187(95)00008-9.

[21] P. Boccotti, Caisson breakwaters embodying an OWC with a small opening - Part I: Theory, Ocean Engineering 34 (5-6) (2007) 806–819. doi:10.1016/j.oceaneng.2006.04.006.

[22] G. Malara, F. Arena, Analytical modelling of an U-Oscillating Water Column and performance in random waves, Renewable Energy 60 (2013) 116–126. doi:10.1016/j.renene.2013.04.016.
URL http://dx.doi.org/10.1016/j.renene.2013.04.016

[23] I. Morrison, C. Greated, Oscillating water Column Modelling, in: Coastal Engineering Proceedings, Vol. 1, 1992, pp. 502–511.

[24] I. Lopez, A. Castro, G. Iglesias, Hydrodynamic performance of an oscillating water column wave energy converter by means of particle imaging velocimetry, Energy 83 (2015) 89–103. doi:10.1016/j.energy.2015.01.119.

[25] K. Ram, M. Faizal, M. Rafiuddin Ahmed, Y.-H. Lee, Experimental studies on the flow characteristics in an oscillating water column device, Journal of Mechanical Science and Technology 24 (10) (2010) 2043–2050. doi:10.1007/s12206-010-0621-z.

[26] M. Folley, T. Whittaker, Validating a spectral-domain model of an OWC using physical model data, International Journal of Marine Energy 2 (2013) 1–11. doi:10.1016/j.ijome.2013.05.003.
URL http://dx.doi.org/10.1016/j.ijome.2013.05.003

[27] I. López, B. Pereiras, F. Castro, G. Iglesias, Optimisation of turbine-induced damping for an OWC wave energy converter using a RANS-VOF numerical model, Applied Energy 127 (2014) 105–114. doi:10.1016/j.apenergy.2014.04.020.

[28] A. Iturrioz, R. Guanche, J. Lara, C. Vidal, I. Losada, Validation of OpenFOAM for Oscillating Water Column three-dimensional modeling, Ocean Engineering 107 (2015) 222–236. doi:10.1016/j.oceaneng.2015.07.051.
URL http://linkinghub.elsevier.com/retrieve/pii/S0029801815003649

[29] I. Simonetti, L. Cappietti, H. El Safti, H. Oumeraci, Numerical Modelling of Fixed Oscillating Water Column Wave Energy Conversion Devices: Toward Geometry Hydraulic Optimization, in: Proceedings of the ASME 34th International Conference on Ocean, Offshore and Arctic Engineering OMAE2015, 2015. doi:10.1115/OMAE2015-42056.
URL http://www.scopus.com/inward/record.url?eid=2-s2.0-84947724837{&}partnerID=tZOtx3y1

[30] P. Boccotti, Comparison between a U-OWC and a conventional OWC, Ocean Engineering 34 (5-6) (2007) 799–805. doi:10.1016/j.oceaneng.2006.04.005.

[31] T. Vyzikas, S. Deshoulières, O. Giroux, M. Barton, D. Greaves, Numerical study of fixed Oscillating Water Column with RANS-type two-phase CFD model, Renewable Energy(Under second revision).

[32] K. Günaydin, M. S. Kabdali, Investigation of Π-type breakwaters performance under regular and irregular waves, Ocean Engineering 34 (7) (2007) 1028–1043. doi:10.1016/j.oceaneng.2006.03.015.

[33] P. Boccotti, Design of breakwater for conversion of wave energy into electrical energy, Ocean Engineering 51 (2012) 106–118. doi:10.1016/j.oceaneng.2012.05.011.

[34] P. Boccotti, P. Filianoti, V. Fiamma, F. Arena, Caisson breakwaters embodying an OWC with a small opening-Part II: A small-scale field experiment, Ocean Engineering 34 (5-6) (2007) 820–841. doi:10.1016/j.oceaneng.2006.04.016.

[35] F. Arena, A. Romolo, G. Malara, A. Ascanelli, S. Ghiretti, A New U-OWC Device to Produce Electrical Power from Ocean Waves : Some Applications to Italian Coasts, in: ICE Conference Coasts, Marine Structures and Breakwaters 2013, Edinburgh, UK, 2013.

[36] K. Ümit Monk, Forecasting for control and environmental impacts of wave energy converters, Ph.D. thesis (2015). doi:10.1029/2003GL016963.

[37] P. R. Teixeira, D. P. Davyt, E. Didier, R. Ramalhais, Numerical simulation of an oscillating water column device using a code based on Navier Stokes equations, Energy 61 (2013) 513–530. doi:10.1016/j.energy.2013.08.062.
URL http://linkinghub.elsevier.com/retrieve/pii/S0360544213007512

[38] P. M. Koola, M. Ravindran, P. A. A. Narayana, Model Studies of Oscillating Water Column Wave-Energy Device, Journal of Energy Engineering 121 (1) (1995) 14–27. doi:10.1061/(ASCE)0733-9402(1995)121:1(14).

[39] Coastal, Ocean and Sediment Transport (COAST) Laboratory, [Online accessed 04-September-2015].
URL http://www.plymouth.ac.uk/coast

[40] G. Payne, Guidance for the experimental tank testing of wave energy converters, Tech. rep. (2008).
URL http://www.supergen-marine.org.uk/drupal/files/reports/WEC_tank_testing.pdf

[41] The wells air turbine for wave energy conversion.

[42] F. He, Z. Huang, Hydrodynamic performance of pile-supported OWC-type structures as breakwaters: An experimental study, Ocean Engineering 88 (2014) 618–626. doi:10.1016/j.oceaneng.2014.04.023.
URL http://linkinghub.elsevier.com/retrieve/pii/S0029801814001620

[43] A. Kamath, H. Bihs, Øivind A. Arntsen, Numerical modeling of power take-off damping in an Oscillating Water Column device, International Journal of Marine Energy 10 (2015) 1–16. doi:10.1016/j.ijome.2015.01.001.
URL http://dx.doi.org/10.1016/j.ijome.2015.01.001

[44] P. Frigaard, M. Christensen, An absorbing wave-maker based on digital filters, in: Coastal Engineering Conference. Proceedings of The International Conference 1, pp. 168–180.

[45] M. E. McCormick, Ocean Wave Energy Conversion, Dover Publications, 2007.

[46] L. H. Holthuijsen, Waves in Oceanic and Coastal Waters, Cambridge University Press, 2007.

[47] K. Hasselmann, T. P. Barnett, E. Bouws, H. Carlson, D. E. Cartwright, K. Enke, J. A. Ewing, H. Gienapp, D. E. Hasselmann, P. Kruseman, A. Meerburg, P. Muller, D. J. Olbers, K. Richter, W. Sell, H. Walden, Measurements of Wind-Wave Growth and Swell Decay during the Joint North Sea Wave Project (JONSWAP), Ergnzungsheft zur Deutschen Hydrographischen Zeitschrift Reihe A(8) (12) (1973) p.95. doi:citeulike-article-id:2710264.

[48] Channel Coastal Laboratory, [Online accessed 04-April-2015].
URL http://www.channelcoast.org/

[49] M. F. P. Lopes, Experimental development of offshore wave energy converters, Ph.D. thesis, Instituto Superior Tecnico (2011).

[50] T. E. Baldock, D. J. Simmonds, Separation of incident and reflected waves over sloping bathymetry, Coastal Engineering 38 (3) (1999) 167–176. doi:10.1016/S0378-3839(99)00046-0.

[51] R. Takaramoto, M. Kashiwagi, K. Sakai, Wave Energy Absorption in Irregular Waves by a Floating Body Equipped with Interior Rotating Electric-Power Generator, Journal of Ocean and Wind Energy 1 (3) 129–134.

[52] D. Carter, Estimation of wave spectra from wave height and period (1982).
URL http://eprints.soton.ac.uk/14556/